GEOPHYSICS, VOL. 63, NO. 1 (JANUARY–FEBRUARY 1998); P. 171—183, 11 FIGS.

Elastic wave velocities during evaporative drying

David Goertz* and Rosemary Knight‡

ABSTRACT

Laboratory measurements of drying rates and elastic wave velocities are made on limestone, dolomite, and sandstone samples during evaporative drying. The drying rate data are very similar in form. There is a constant rate period at higher saturations and a falling rate period below saturation levels of approximately 0.2. The falling rate period marks the transition in the sample from hydraulically connected to disconnected water. There is a strong link between elastic wave velocities and the drying process because different pore geometries drain at different stages in drying. The drainage of these different geometries results in specific changes in the moduli and velocities.

Simple models of the pore geometries and the drying process are used to model the velocity data. The velocity-saturation relationship for each of the three samples is very different in form because of differences in pore-space microgeometry. Of particular interest is the velocity response during the falling rate period of drying. In the limestone and the sandstone, there is a significant decrease in bulk and shear moduli and elastic wave velocities because of the drainage of crack-like pores and grain contacts. In contrast, the absence of these pore geometries in the dolomite results in essentially no changes in the moduli at low saturations. An understanding of the drying process and resulting pore-scale fluid distribution provides useful insights into the observed form of the velocity-saturation relationship.

INTRODUCTION

Elastic wave velocities measured in porous rocks during laboratory experiments have been found to be sensitive to the distribution of the fluids in the pore space (Knight and Nolen-Hoeksema, 1990; Cadoret et al., 1992a). The pore-scale fluid distribution is, in turn, determined by the microgeometry of the pore space, the interfacial free energies in the system, and the past fluid displacement processes or saturation history of the rock.

In this study, we are interested in the process of evaporative drying, the resulting fluid distributions, and the corresponding dependence of elastic wave velocities on saturation levels. Evaporative drying is the main process responsible for the reduction of water saturation at the earth's surface and should be considered in the accurate interpretation of elastic wave velocity data from the near surface. In addition, laboratory measurements of elastic wave velocities may prove to be a useful way of obtaining information about fluid distribution and connectivity in porous samples during drying. We measure the elastic wave velocities and drying rates of three samples, limestone, dolomite, and sandstone, during evaporative drying. We find that an understanding of the way in which the drying process and the pore-space microgeometry interact is of importance when interpreting the form of the velocity-saturation relationship.

The drying process

There has been little discussion in the geophysical literature about the nature of fluid distribution in rocks during evaporative drying. In fields such as chemical engineering and soil science, the drying process has been the subject of a considerable amount of research. The following summary of material relevant to our study is based primarily on the works of Whitaker (1985), Keey (1972), and van Brakel (1980).

Drying is a specific form of drainage in which liquid water is replaced by air through evaporation. Information about the drying process in a porous material can be obtained from the drying rate curve, shown schematically in Figure 1. The form of the plot in Figure 1 is representative of what is observed for rigid porous materials with most pores being greater than 1 μm in diameter (e.g., porous sedimentary rocks). There is an initial drop in drying rate as the level of water saturation S_w decreases, followed by a constant rate period, and finally a falling rate period at lowest saturations. The variation in drying rate is caused

Published on "Geophysics Online" June 12, 1997. Manuscript received by the Editor August 25, 1995; revised manuscript received February 21, 1997.
*Formerly Department of Geophysics and Astronomy, University of British Columbia, Vancouver, British Columbia, Canada; presently Imaging Research, Research Bldg., Sunnybrook Health Sciences Centre, North York, Ontario, Canada M4N 3M5. E-mail: goertz@pooh.sunnybrook.utoronto.ca.
‡Department of Geological Sciences, University of British Columbia, Vancouver, British Columbia, Canada. E-mail: knight@geop.ubc.ca.
© 1998 Society of Exploration Geophysicists. All rights reserved.

by changes in the dominant mass transport process, which in turn is related to the distribution and connectivity of the water. The two primary mechanisms responsible for mass transport are capillary transport in the liquid phase and diffusion in the vapor phase. Capillary transport results from a hydraulic pressure gradient within the sample. Diffusion, a much slower process, is driven by a gradient in the concentration of water vapor.

When drying is first initiated, water-air menisci form in the surface pores and evaporation begins from the sample surface. The removal of heat from the surface water to provide the latent heat for vaporization causes the decrease in drying rate that is often seen at highest saturations. At this stage, the mass transport process that is dominant throughout the constant rate period is established. As the water-air menisci enter the sample, liquid water is drawn through capillary transport to the sample surface, where it evaporates. The rate-controlling step is the diffusion and/or convection of vapor from the surface of the sample into the surrounding environment. Throughout the constant rate period, as water-air menisci penetrate the pore structure, both fully saturated and partially saturated pores are present. The key feature of this period is a high degree of hydraulic connectivity that allows the supply of liquid water to the sample surface to balance the rate of evaporation, resulting in a constant, or relatively constant, rate. There is some diffusion of water vapor from within the sample to the surface, but this diffusion is considered to be negligible.

As drying progresses, the connectivity of the liquid phase within the sample is reduced to the point at which the capillary flow of liquid to the surface can no longer balance the rate of evaporation from the surface. The saturation of the surface layer of the sample is rapidly reduced, and the drying rate enters the final falling rate period. Although the exact transport conditions during the falling rate period are not well understood, it is generally accepted that there is a transition from capillary transport to vapor-phase diffusion. This change in dominant mechanism is linked to the continued decrease in hydraulic connectivity. The loss of hydraulic connectivity as a sample enters the falling rate period has led to the suggestion that the beginning of the falling rate period indicates the approach of the sample to a state of irreducible water saturation (Whitaker, 1985).

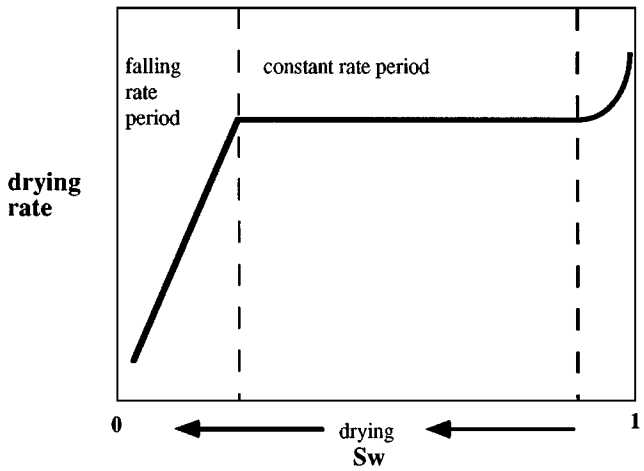

FIG. 1. Schematic drying rate curve for a porous material as the level of water saturation S_w decreases during evaporative drying.

Sample-scale heterogeneity in saturation level can develop in samples during drying. During the final falling rate period, saturation heterogeneity related to the geometry of the sample is assumed to exist in most porous materials, with the outside of the sample being less saturated than the inside of the sample. As a result, the water in the pore space toward the outside can be hydraulically disconnected, whereas the water toward the inside still maintains a high level of hydraulic connectivity. Both Guillot et al. (1989), using magnetic resonance imaging, and Cadoret et al. (1992b), using X-ray tomography, observed such saturation heterogeneity at low saturation levels ($S_w < 0.15$). Cadoret et al. (1992a) also found saturation heterogeneity at very high saturation levels ($S_w > 0.95$), again with the outside being less saturated than the inside. Between these saturation extremes, the fluid distribution appears to be controlled only by the intrinsic properties of the rock sample, not by the sample geometry (Cadoret et al., 1992b).

What is clear from a review of the literature is that there is not yet a complete understanding of the physical processes that occur during drying, and a number of questions are unanswered regarding the specific time-dependent behavior that is observed. The main objective of this study is to use what is presently known about the interpretation of drying rates, as summarized above, to obtain information about pore-scale fluid distribution in rock samples during evaporative drying. Our interpretation of fluid distributions is then used to assist in understanding and modeling the observed forms of the velocity-saturation relationship for the three porous rock samples.

Modeling velocity-saturation relationships

Elastic wave velocities in a homogeneous isotropic medium can be expressed in terms of the bulk modulus (K), shear modulus (μ), and density (ρ), written as

$$V_P = \sqrt{\frac{K + \frac{4}{3}\mu}{\rho}}, \tag{1}$$

$$V_S = \sqrt{\frac{\mu}{\rho}}, \tag{2}$$

where V_P is the compressional-wave velocity and V_S is the shear-wave velocity. The main effect of pore fluids on elastic wave velocities is caused by the bulk properties of the fluids and the contribution to the elastic response of the pore space. A second effect, which is seen only at low levels of water saturation, is caused by rock-water interactions. In addition to these two pore-scale effects, sample-scale heterogeneity in fluid saturation may need to be considered.

The extent to which the bulk properties of fluids affect the elastic moduli of a rock depends upon the nature of the porosity and the frequency of the elastic waves. Because of heterogeneities in pore shape, orientation, and saturation, the passage of an elastic wave can induce pore-scale pressure gradients that cause local flow (O'Connell and Budiansky, 1974, 1977; Mavko and Nur, 1979). At low frequencies, local flow occurs and such pore-scale pressure gradients can be dissipated. At

high frequencies, viscous and inertial effects within the fluid become significant and inhibit local fluid flow (Murphy et al., 1986; Mavko and Jizba, 1991). The pore fluid is "unrelaxed" and exerts pressure on the pore wall that acts to stiffen the frame moduli. As a consequence, velocities measured at ultrasonic frequencies tend to be higher than those measured at seismic frequencies (Winkler, 1985) and can be sensitive to the saturation state of individual pores (Endres and Knight, 1989; Knight and Nolen-Hoeksema, 1990). The stiffening effect of pore fluids in individual pores depends upon pore geometry, with the moduli being most sensitive to the saturation state of thin compliant regions of the pore space (Walsh, 1965).

It is this link between ultrasonic elastic wave velocities and the location of the water, relative to pore geometry, that we want to consider for the process of evaporative drying. Laboratory measurements of drying rates and elastic wave velocities are made on three samples, and the results are modeled using the numerical routine of Endres and Knight (1989). This approach builds on the models developed by Kuster and Toksöz (1974) and Toksöz et al. (1976), in which the mechanical behavior of a porous rock is modeled by representing the pore space as oblate spheroidal inclusions in a homogeneous background solid. Pores are described in terms of the aspect ratio of the inclusions, where the aspect ratio α is defined as the ratio of the length of the semiminor axis to that of the semimajor axis. The model of Endres and Knight (1989) allows the saturation state of individual pores with specific aspect ratios to be controlled and incorporates the rigidity contribution of the pore fluids. In this way, a wide range of velocity-versus-saturation relationships can be explored for various saturation processes.

The model that is used in this study does make two significant approximations. The first is that rock pores, which are often very geometrically complex, can be described by idealized ellipsoidal inclusions. As a first-order approximation, however, much of the mechanical behavior of a rock can be investigated with this type of model. It is also assumed that it is the saturation state of individual pores that dominates the elastic behavior of the rock and that communication of fluids between pores during the passage of elastic waves can be neglected. At ultrasonic frequencies, at which viscous and inertial effects become significant, this is a valid assumption, and this type of model has been found to produce reasonable results in fully saturated rocks (Toksöz et al., 1976) and in partially saturated sandstone (Endres and Knight, 1991).

A second type of effect that the presence of pore fluids can have on elastic wave velocities has been observed at low saturations, at which the presence of a small amount of water wetting the internal surfaces of a rock can lower the elastic moduli of a dry rock (Born and Owen, 1935; Wyllie et al., 1962; Pandit and King, 1979; Clark et al., 1980; Murphy et al., 1984). In sandstones, this effect corresponds to the presence of three or four monolayers of adsorbed water (Knight and Dvorkin, 1992) and is caused by the weakening of grain contacts (Murphy et al., 1984). Such an effect has been observed in some carbonates (Clark et al., 1980), but the mechanism is not understood. These rock-fluid interface effects will be observed only in the final stages of drying, when surface-adsorbed water is removed, and will be considered in interpreting the data.

The above discussion of the velocity-saturation relationship has focused on the role of pore-scale fluid distribution. As noted in the description of the drying process, sample-scale heterogeneity in saturation level can develop during the falling rate period. If the scale of heterogeneity approaches or exceeds the elastic wavelength, then measured velocities can be affected by wave-path dispersion (Cadoret et al., 1993). This possibility will be considered in the interpretation of our data.

EXPERIMENTAL PROCEDURE AND RESULTS

Pore geometry is a primary factor influencing both the sensitivity of velocities to saturation level and the distribution of fluids during drying. As a result, pore geometry is a key link between the drying process and the corresponding velocities. For this study, we therefore selected three samples with very different pore geometries: limestone, dolomite, and sandstone. The petrographic description of each sample is used to construct a simplified model of the pore space in which the pore space of each rock is represented by a concentration of ellipsoidal pores with varying aspect ratios. Drying rate data are collected for each sample and used to obtain information about the distribution of water in the samples at various levels of saturation. This fluid distribution information is then used with the pore-space models to explain the observed changes in elastic moduli and wave velocities during evaporative drying. Additional data collected during the adsorption of water in the sandstone sample are used to examine the effects of water on elastic behavior at very low saturations and to assess the importance of saturation heterogeneity at these saturations.

Sample description

The cylindrical samples used in the study are 25 mm in diameter and range in length from 25 mm to 38 mm. The same samples were used to obtain drying rates and to measure elastic wave velocities. Sample porosities were calculated using the measured mass of water present in the water-saturated sample. A description of the pore-space microgeometry of each sample was based on thin-section analysis (Wilks and Tercier, 1993). Because we model elastic wave velocities using the numerical approach of Endres and Knight (1989), we are most interested in describing the pore space in terms of aspect ratios and concentrations.

The limestone sample is composed of calcite grains ranging in size from 0.008 to 0.21 mm. There is a random distribution of subrounded macroscopic pores that range in size from 0.1 mm to 1 mm, with most pores being between 0.5 mm and 1 mm. These macropores are interconnected commonly by fracture porosity of a very low aspect ratio. The limestone sample has a porosity of 0.139 and a permeability, measured by Shell Canada, of 2.25 mD.

The dolomite sample used in this study is Baker dolomite, which is a crystalline carbonate composed of carbonate grains ranging in size from 0.06 mm to 0.3 mm. The pores range in size from 0.02 mm to 0.3 mm, with aspect ratios ranging from approximately 0.1 to 1. No fracture or crack-like porosity is evident; the grains appear to be well cemented from the dolomitization process. The porosity of this sample is 0.234, and the permeability, measured by Shell Canada, is 104 mD.

The sandstone sample is Berea 300, a quarried sandstone, composed primarily of quartz grains with approximately 5% clay. The pores range in size from about 0.02 mm to 0.2 mm and

in aspect ratio from approximately 0.1 to 1. As noted in previous studies (e.g., Murphy et al., 1986), a significant amount of crack-like (low-aspect-ratio) porosity is evident in this sandstone at grain boundaries. The porosity of the Berea 300 sample is 0.23. The number 300 refers to the approximate permeability of the sample in millidarcies, as determined by air permeability measurements at the quarry.

Drying rates: Procedure and results

Drying rate data were obtained by placing a saturated sample on a weigh scale under ambient laboratory conditions. Samples were saturated by evacuation in a pressure chamber, introducing degassed, distilled water into the sample chamber and pressurizing the water to 14 MPa overnight. The scale was interfaced with a computer, and weight measurements, used to calculate S_w, were made at regular time intervals until the sample weight no longer decreased.

The drying rate data for the each of the samples, shown in Figure 2, are all qualitatively similar in form. An initial decrease in rate is evident, and this is followed by a period of relatively constant drying rate. At values of S_w around 0.20, the samples begin to enter the falling rate period. During collection of the drying rate data, we did not control temperature or humidity. Since the drying rate during the constant rate period can be influenced by ambient conditions, this means that the actual magnitude of the drying rate contains no usable information. Also, for any given sample, we noted some fluctuations in the rate and a slight decrease in the rate throughout the constant rate period. The slight decrease most likely is the result of an increase in humidity immediately adjacent to the sample surface during drying.

Measurement of elastic wave velocities: Procedure and results

The elastic wave velocities V_P and V_S were measured in the samples using an ultrasonic pulse transmission method. This method involves using one transducer as a wave source and one as a receiver. Traveltimes, determined by selecting first-arrival times, are used to calculate velocities. The transducers are capable of transmitting either compressional or shear waves. Compressional waves, centered at 500 kHz, are generated by pulsing a large axially oriented crystal. Shear waves, centered at 400 kHz, are generated by pulsing an arrangement of eight azimuthally oriented crystals.

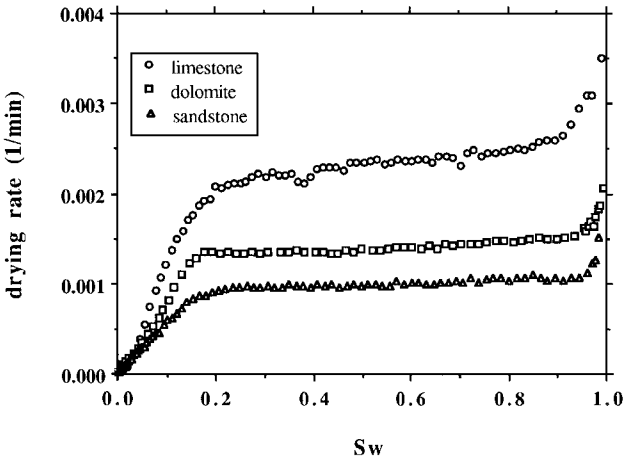

FIG. 2. Drying rates of the three samples versus S_w. These data were collected during evaporative drying.

For the collection of the velocity data during evaporative drying, we started with a fully water-saturated sample. Velocity measurements began immediately after the sample was removed from the saturating chamber, and S_w was reduced through evaporative drying under ambient laboratory conditions. At low levels of saturation (S_w less than approximately 0.05), S_w was reduced by placing the samples in a desiccator. The "dry," or zero-saturation, measurements were made on samples that had been heated at 60°C for 1 day and cooled in a desiccator.

We were able to investigate in detail the variation in velocities at low saturation levels in the sandstone sample by starting with a dry sample and increasing S_w through the adsorption of water vapor. The dry sample was placed on a stand in a closed chamber that was partially filled with distilled water, thereby exposing it to air with a relative humidity close to 100%. Attempts to collect data from the carbonate samples using this method were unsuccessful; the samples did not adsorb much water, and there was overwhelming scatter in the small amount of collected data.

The data for the three samples are presented as plots of V_P (Figure 3), K (Figure 4), V_S (Figure 5), and μ (Figure 6) as a function of S_w. The data for the limestone and dolomite samples are combined on single plots in Figures 3a, 4a, 5a, and 6a. The plots for the sandstone sample in Figures 3b, 4b, 5b, and 6b contain data collected during evaporative drying and during adsorption of water vapor.

For the limestone sample, Figures 3a and 4a show a gradual decrease in V_P and K as S_w is reduced from 1.0 to a value of approximately 0.15. In this same saturation range, μ (Figure 6a) remains relatively constant, resulting in an increase in V_S with decreasing S_w (Figure 5a) because of a density effect. In all the velocity and moduli data, there is a significant change in saturation dependence at an S_w of approximately 0.15: Further reduction in S_w causes a rapid decrease in moduli and velocities with decreasing S_w. We note that this saturation corresponds to the region of transition from the constant rate period to the falling rate period in the drying rate data for this sample (Figure 2).

For the dolomite sample, there are no data for moduli at the highest saturations because signal attenuation caused poor-quality shear-wave data above a saturation level of 0.85. The velocity data are distinctly different from the limestone data in the form of the dependence on S_w. As shown in Figure 3a, most of the changes in V_P occur in the higher saturation range, not at low saturations, as in the limestone data. The V_P of the dolomite decreases steadily as S_w decreases from 1.0 to approximately 0.50 and then stays relatively constant at lower saturations. A similar form of dependence on S_w is seen for K (Figure 4a). In Figure 5a, V_S shows very little sensitivity to S_w, compared to that seen in V_S for the limestone sample. The gradual increase in V_S is caused primarily by a density effect, as can be seen by the relatively constant shear modulus in Figure 6a.

When we consider the drying rate data for the dolomite sample, it is interesting to note that at $S_w = 0.5$, at which the dependence of V_P on S_w changes significantly, there is no corresponding change in the drying rate data. In the drying rate data, the transition to the falling rate period occurs at approximately $S_w = 0.15$; this finding is not reflected in the velocity

data. There is a subtle variation in μ below this saturation, but given the scatter in the shear-wave data, we cannot attribute much significance to this behavior.

In reviewing the data for the Berea 300 sample, let us first consider data collected during evaporative drying. In the P-wave data in Figure 3b, four distinct regions in saturation dependence can be identified . Within the first region, at the highest saturation levels, there is a decrease in V_P as S_w decreases from 1 to approximately 0.4. In the second region, defined as $0.15 < S_w < 0.4$, V_P shows little change with decreasing S_w. In the third region, defined as $0.05 < S_w < 0.15$, there is a large decrease in V_P with decreasing S_w. As S_w is decreased further toward zero in the fourth region, V_P increases to reach the value for the dry rock. The form of the dependence of V_P on S_w is also seen in the variation of K with S_w (Figure 4b). The variations in V_S and μ seen in Figures 5b and 6b also can be divided into four regions; the relative magnitudes of the changes in these regions are different from those for V_P. V_S and μ decrease with S_w in the upper ranges of saturation, then μ remains relatively constant and V_S shows a gradual increase with saturation. As S_w is reduced below 0.15 there is a small decrease in V_S followed by a sharp increase.

For the Berea 300 sample, we see noticeable differences between the data collected during adsorption and those collected during drying. As S_w is increased from the dry state through the adsorption of water, the elastic wave velocities and the moduli decrease substantially. This response is followed by an increase of similar magnitude in the measured parameters until the point of maximum adsorption at $S_w = 0.15$. A comparison of the two data sets when we model the velocity variation will allow us to assess the effect of saturation heterogeneities on the velocity data.

When we compare the form of the Berea velocity data to the drying rate data, we see that the transition to the falling rate

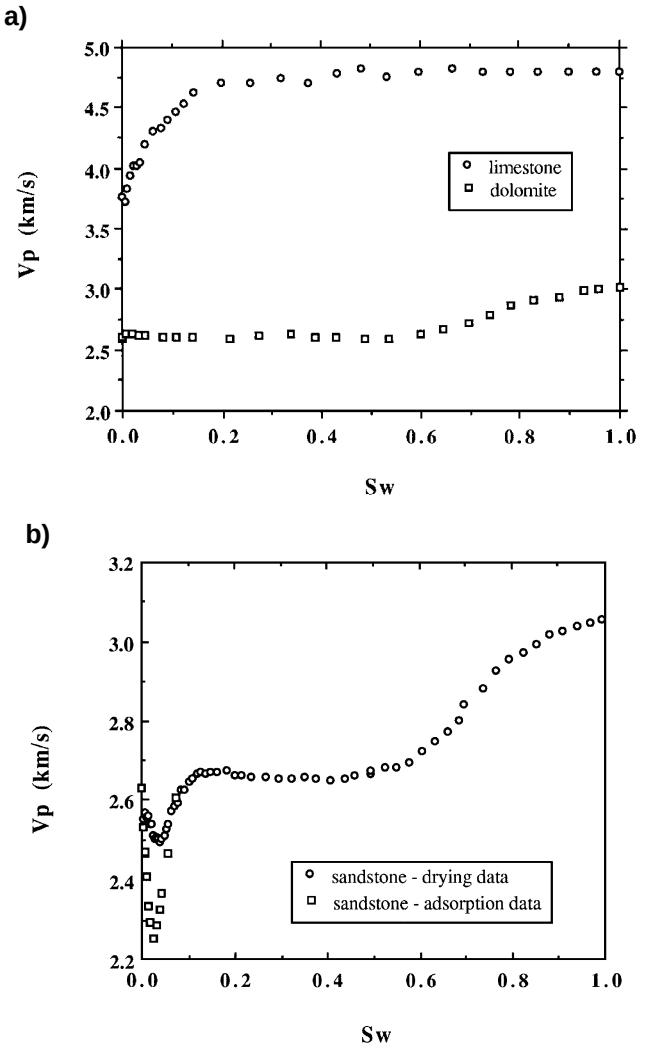

FIG. 3. (a) V_P versus S_w data obtained for the limestone and dolomite samples through the measurement of elastic wave velocities during evaporative drying. (b) V_P versus S_w data obtained for the sandstone sample through the measurement of elastic wave velocities during evaporative drying and during the adsorption of water vapor.

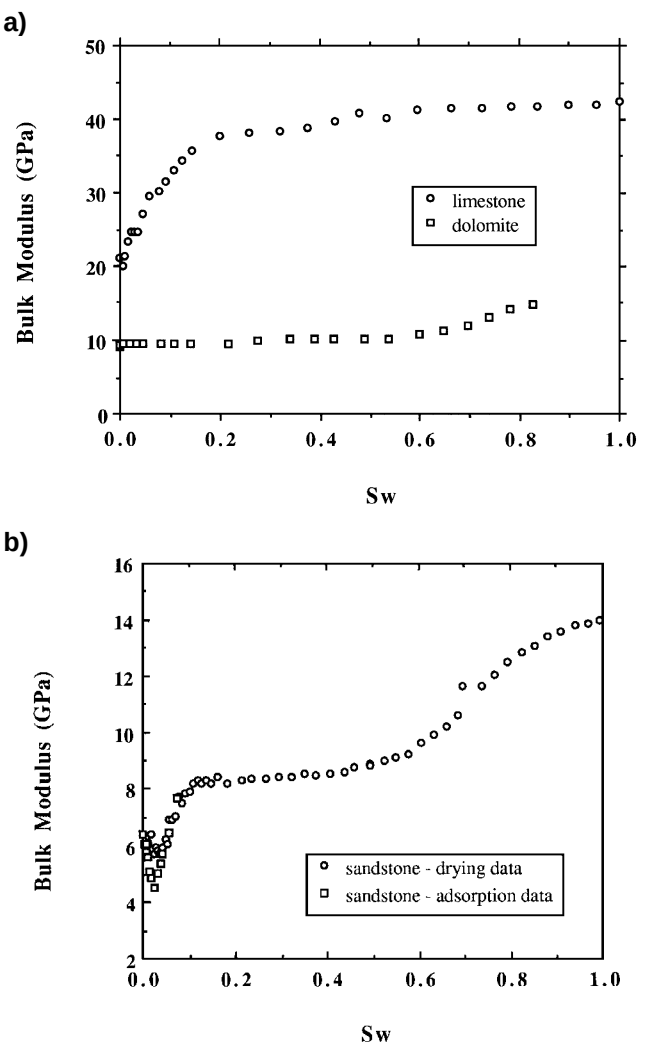

FIG. 4. (a) Bulk modulus versus S_w data obtained for the limestone and dolomite samples through the measurement of elastic wave velocities during evaporative drying. (b) Bulk modulus versus S_w data obtained for the sandstone sample through the measurement of elastic wave velocities during evaporative drying and during the adsorption of water vapor.

period in the drying rate curve (Figure 2) occurs near $S_w = 0.2$. In the velocity data, we observe changes in the form of the saturation dependence at S_w values of approximately 0.4, 0.15, and 0.05. In our three samples, therefore, we see considerable variations in the form of the velocity-saturation relationship and in the correspondence with the drying rates. These variations can be explained by considering the differences in pore-space microgeometries.

FLUID DISTRIBUTION FROM DRYING RATE DATA

The drying rate data can be used to obtain information about fluid distributions at two scales, the sample scale and the pore scale. Both of these scales can be expected to affect the velocity-saturation relationship.

Let us first consider sample-scale fluid distribution. Heterogeneity in saturation levels can affect elastic wave velocities if the scale of the heterogeneity approaches or exceeds the wavelength λ of the elastic wave; for our samples, λ ranges from 3 to 5 mm. In all the samples, we can clearly recognize the transition from the constant rate period to the falling rate period. It is well established that during the falling rate period, sample-scale saturation heterogeneity will evolve. Therefore, we assume that the scale of saturation heterogeneity in the falling rate period is large enough that it could affect the measured velocities. Above that saturation, throughout the constant rate period, Cadoret et al. (1992a and b) found that if the scale of the porous network is sufficiently less than λ, then the saturation distribution can be considered effectively homogeneous. In the sandstone and dolomite samples, the maximum pores observed in thin sections range from 0.1 to 0.4 mm, an order of magnitude less than λ. In the limestone sample, some pores were found to be as large as 1 mm but still less than λ. In our modeling of the velocity data, we therefore assume for all samples that pore-scale effects dominate the elastic behavior throughout the constant

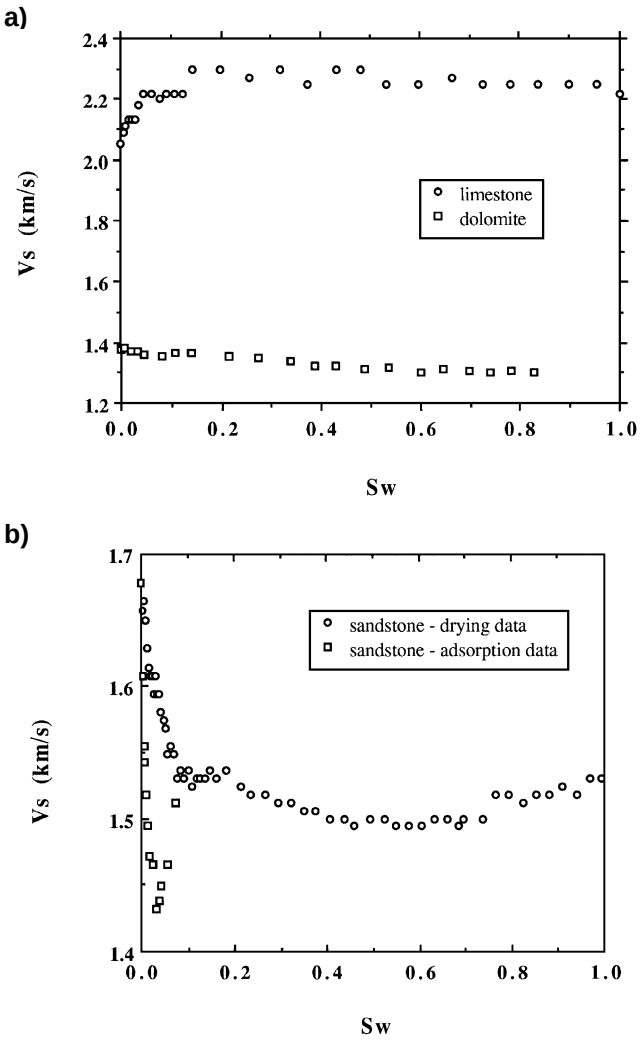

FIG. 5. (a) V_S versus S_w data obtained for the limestone and dolomite samples through the measurement of elastic wave velocities during evaporative drying. (b) V_S versus S_w data obtained for the sandstone sample through the measurement of elastic wave velocities during evaporative drying and during the adsorption of water vapor.

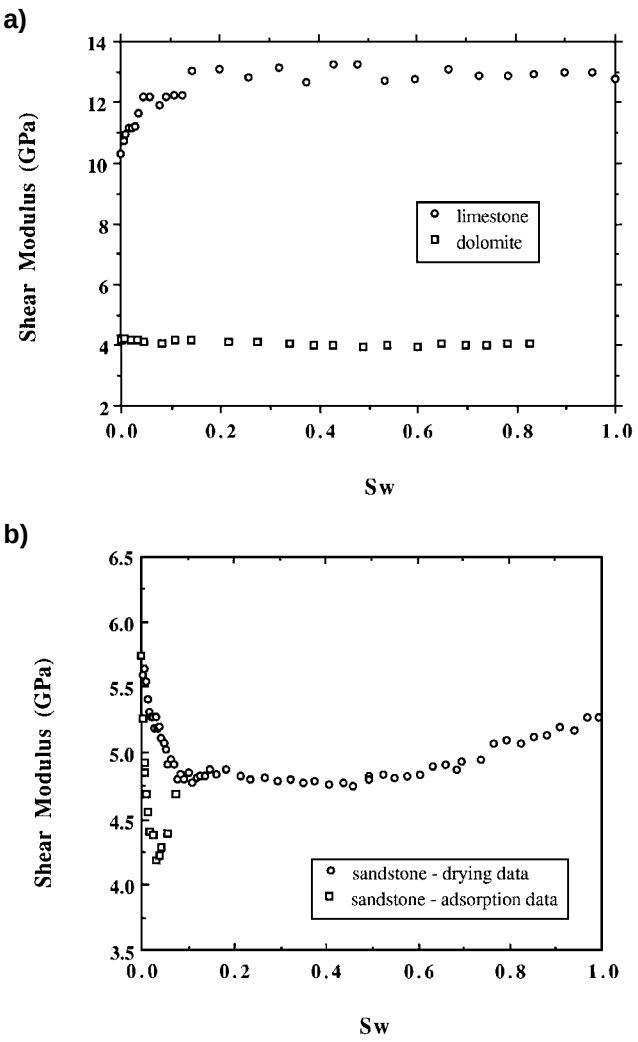

FIG. 6. (a) Shear modulus versus S_w data obtained for the limestone and dolomite samples through the measurement of elastic wave velocities during evaporative drying. (b) Shear modulus versus S_w data obtained for the sandstone sample through the measurement of elastic wave velocities during evaporative drying and during the adsorption of water vapor.

rate period, and we consider sample-scale saturation heterogeneity only within the falling rate period.

In terms of characterizing pore-scale fluid distribution, the transition to the falling rate period is an important saturation range because it indicates that the water in the sample is going from a hydraulically connected state to a hydraulically disconnected state. Of specific relevance to our study is the fact that water in the hydraulically disconnected state is preferentially retained in certain pore geometries. The tendency of certain pores to retain water can be quantified by considering the capillary pressure, which is the pressure difference across the water-air meniscus. Water will be retained in regions of high capillary pressure. In a cylindrical pore with radius r, assuming that the water perfectly wets the solid surface, the capillary pressure P_C, is described by

$$P_C = P_W - P_A = \frac{2\sigma_{AW}}{r}, \tag{3}$$

where P_W and P_A are the pressures in the water and the air, respectively, and σ_{AW} is the surface tension at the air-water interface. From expression (3), it can be seen that the water will preferentially occupy pores of smaller radii while pores of larger radii will drain. Although the pore geometries of the rocks that we are examining in this study do not resemble capillary tubes and although the topology of the pore space may affect the order of drainage of pores, we can assume that large pores are the first to drain while small pores retain water.

A second geometry, which illustrates how a granular rock retains water, is a pendular ring of water held in the region of contact between two spherical grains. The capillary pressure across the air-water interface can be described by

$$P_C = \sigma_{AW}\left(\frac{1}{r_1} + \frac{1}{r_2}\right), \tag{4}$$

where r_1 and r_2 are the two principle radii of curvature that describe the shape of the meniscus. As r_1 and r_2 decrease in magnitude, reflecting a lower saturation level, the capillary pressure will increase and the liquid will become more tightly held. Therefore, at low saturations, we also expect to find water held as pendular rings at grain contacts.

A third geometry that is of interest is that of water held in the region between two parallel plates, with air at the boundaries; such a geometry approximates crack-like pores in rocks. Assuming that the lines of contact between the water and the bounding air are straight, then the capillary pressure in the liquid phase is

$$P_C = P_W - P_A = \frac{\sigma_{AW}}{d}, \tag{5}$$

where d is the separation distance between the plates. Because in rocks the separation between crack faces can be very small, the capillary pressure is very high in such regions, leading to the retention of water in these types of pore geometries.

In addition to water being retained in regions of the pore space in which the capillary pressure is high, water also will remain coating the solid internal surfaces of the pore space. A few monolayers of water are adsorbed onto the solid surface through a combination of van der Waal's and electrostatic forces and are presumed to be the last water to be removed from a rock during drying. More water also can be retained in the surface roughness where the topography of the surface causes pockets of water to become hydraulically disconnected from the remainder of the bulk water in the pore space.

We propose a very simple link between pore-scale fluid distribution and the drying rate data. Throughout the constant rate period, when there is a high degree of hydraulic connectivity, water that is tightly held in the pore space because of capillary or surface forces will not drain readily. There is a large volume of accessible water in larger pores (i.e., lower capillary pressure) that is much more easily displaced by air. When a porous rock enters the falling rate period, it is well known that there is a reduction in the hydraulic connectivity of the water and that vapor-phase diffusion becomes the dominant mechanism for transporting water to the surface of the sample. At this stage, the water in small pores, at grain contacts, in crack-like geometries, and coating the surfaces starts to drain. The contrasting elastic response of these two types of pore space (those that retain water and those that do not) is the link between the drying process and elastic wave velocity data.

THE LINK TO ELASTIC WAVE VELOCITIES

The main focus of our study is the effect of the bulk properties of the fluid on ultrasonic velocities, which we model using the method of Endres and Knight (1989). During the drying process, the geometry of a pore determines its saturation state. The link to laboratory measurements of elastic wave velocities is the result of the way in which the change in elastic moduli with saturation also is controlled by the geometry of the pores. To illustrate this effect, we use our numerical model to calculate the bulk and shear moduli of pores with various aspect ratios for the dry (air-filled) and saturated (water-filled) cases. The results (Figure 7), as a function of the aspect ratio of the inclusions are expressed in terms of the relative increases in moduli ΔK and $\Delta\mu$ as defined by equations

$$\Delta K = \frac{K_{sat} - K_{dry}}{K_{dry}}, \tag{6}$$

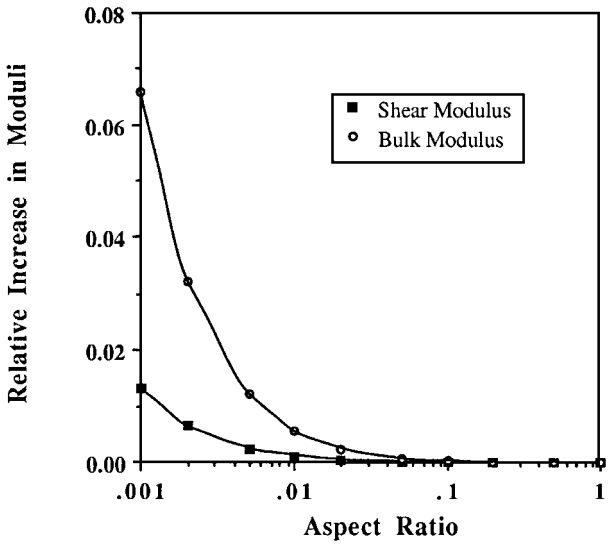

FIG. 7. Relative increases in bulk and shear moduli as the saturation state of the pores is changed from dry (air filled) to saturated (water filled). The relative increase is shown as a function of the aspect ratio of the pores.

and

$$\Delta\mu = \frac{\mu_{sat} - \mu_{dry}}{\mu_{dry}}, \quad (7)$$

where K_{dry} and μ_{dry} are the moduli when the inclusions are air filled and K_{sat} and μ_{sat} are the moduli when the inclusions are water filled. The moduli of the two fluids are $K = 2.1 \times 10^9$ N/m^2 and $\mu = 0$ for water and $K = 1.4 \times 10^6$ N/m^2, $\mu = 0$ for air. From these figures, it can be seen that the moduli of a medium containing low-aspect-ratio pores will be very sensitive to the compressibility of the pore fluids. Replacing air with the much less compressible water causes a large increase in moduli in the low-aspect-ratio inclusions.

It is important to note that the relative increase in the shear modulus is always smaller than that of the bulk modulus. This fact is evident in Figure 8, which shows the ratio of the relative increases in bulk and shear moduli plotted as a function of aspect ratio. From this plot, it can be seen that the shear modulus is not affected at all by the saturation state of spherical pores. As the aspect ratio is decreased, the ratio approaches a constant value, with the relative increase in the shear modulus being approximately 20% that of the bulk modulus. Similar results were obtained by Mavko and Jizba (1991), who showed that both the bulk and the shear moduli can be affected by the saturation state of crack-like compliant porosity. In their study, Mavko and Jizba found that the relative increase in the shear modulus was 26.6% that of the bulk modulus.

For the purposes of our numerical modeling, we consider only the effects associated with the bulk fluids and pore-scale fluid distribution. (Effects associated with the rock-fluid interface and saturation heterogeneity are discussed in a later section with regard to the Berea data for which adsorption data are available at low saturations.) In our modeling, the constant rate period is represented as a saturation range over which all pores become partially drained but maintain a high degree of hydraulic connectivity. This period is followed by a period over which the saturation level in the partially drained pores is reduced further but the liquid remains hydraulically connected. Low-aspect-ratio regions of the pore space (grain contacts and crack-like pores) are assumed to remain saturated throughout the entire constant rate period. For the purposes of this study, it is the form of the velocity-saturation relationship that is of interest. Therefore, given that the pore spectrum characteristics are only qualitatively estimated, the absolute magnitudes of the calculated moduli are not meaningful and therefore are not shown.

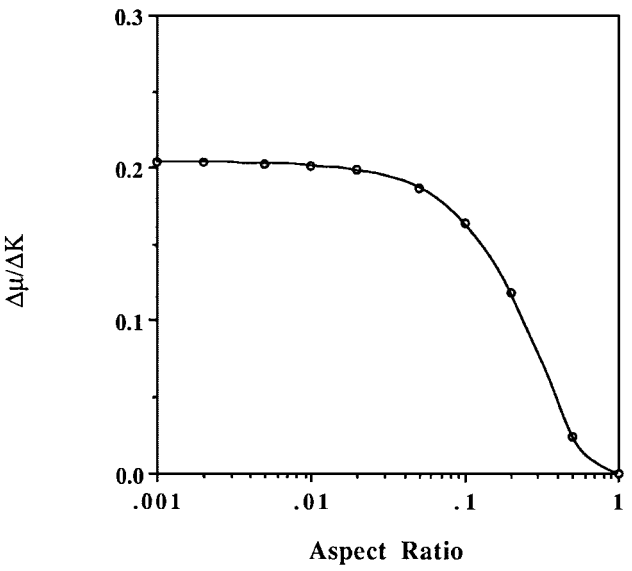

FIG. 8. Ratio of relative increases in bulk and shear moduli as the saturation state of the pores is changed from dry (air filled) to saturated (water filled). The ratio is shown as a function of the aspect ratio of the pores.

Modeling the limestone data

The pore-space model for the limestone sample is composed of a large concentration of high-aspect-ratio inclusions representing the macropores and a small concentration of very-low-aspect-ratio pores representing the fracture porosity or crack-like pores. The proposed model for fluid distributions during drying is shown in Figure 9a as six steps labeled A through F. The corresponding form of the relationship between the moduli and the water saturation level that is produced by such a model is shown in Figure 9b; this figure is labeled with letters to show the link to the steps in Figure 9a.

The drying process can be divided into three main stages. In the first stage, which occurs during the early part of the constant rate period, all macropores are sequentially and partially drained; this stage is shown as steps A to D in Figure 9a. A substantial amount of water is left in the partially drained pores to indicate that the saturation level is high enough for hydraulic connectivity to be maintained. As shown in Figure 9b, there is a gradual decrease in bulk modulus as the macropores are drained to a partial saturation state at the end of step D. The shear modulus is essentially flat in this region, since it is relatively insensitive to the saturation state of high-aspect-ratio pores.

In the second stage (step E in Figure 9a), which lasts until the falling rate period, the saturation level of all the partially saturated macropores is further reduced until only a small amount of hydraulically disconnected surface water remains in these large pores. Both the bulk and the shear moduli are constant during this continued removal of water, shown in Figure 9b as the region between the points labeled D and E. The moduli of a water-filled pore are reduced substantially with the addition of a small amount of compressible air, but the subsequent addition of more air has little effect. At this point, the crack-like pores remain fully water saturated. We emphasize again that with this model, it is assumed that frequencies are high enough for the fluids contained in the crack-like porosity to be unrelaxed and not communicate through fluid flow with the partially drained regions of the pore space.

In the final stage (step F in Figure 9a), the falling rate period, the surface water is removed from the macropores. In our inclusion-based model, the removal of this water has no effect on the moduli. The significant event, in terms of the moduli, is the drainage of the crack-like pores during this final stage. This drainage causes a sharp drop in both the bulk and the shear moduli, shown in Figure 9b between points E and F.

We see good agreement in the form of the model data with the experimental velocity and drying rate data collected for this sample. In the upper ranges of saturation, the macropores drain, causing only a small change in the bulk modulus and

no change in the shear modulus. There is a distinct and pronounced region of decrease in both moduli in the falling rate period that is associated with the removal of water that is held in the crack-like pores. These modulus effects dominate the velocity response, the result being a very simple form of dependence of velocity on saturation. For this sample, there is good correspondence between the drying rate variation with S_w and the velocity variation with S_w.

Modeling the dolomite data

The pore-space microgeometry of the dolomite sample is represented in the model by intermediate- and high-aspect-ratio inclusions. For the purposes of modeling the effects of saturation on moduli, we used the fluid distribution scenario during drying that is shown in Figure 10a. The forms of the modulus-saturation relationships that are produced by this model are shown in Figure 10b, labeled to correspond to the steps in Figure 10a.

In the first stage of drying, which corresponds to the early stages of the constant rate period, all pores are sequentially and partially drained (steps A to D in Figure 10a). The saturation level throughout the constant rate period stays high enough to maintain good hydraulic connectivity. Thus, in the model of the drying process, a significant amount of water is left in the drained pores. As shown in Figure 10b between points A and D, the bulk modulus decreases steadily throughout this saturation range and the shear modulus shows a modest decrease. These decreases are caused by the introduction of air into all pores.

In the second stage (step E), the saturation level in the partially drained pores is reduced toward zero. Since no crack-like (low-aspect-ratio) pores are present, the water retained until low saturations are reached is water held in surface roughness and as an adsorbed layer. The removal of this water in step F has no effect on the moduli. Thus, in contrast to the limestone data, the subsequent and complete drainage of pores in the falling rate period produces no change in the bulk or shear moduli.

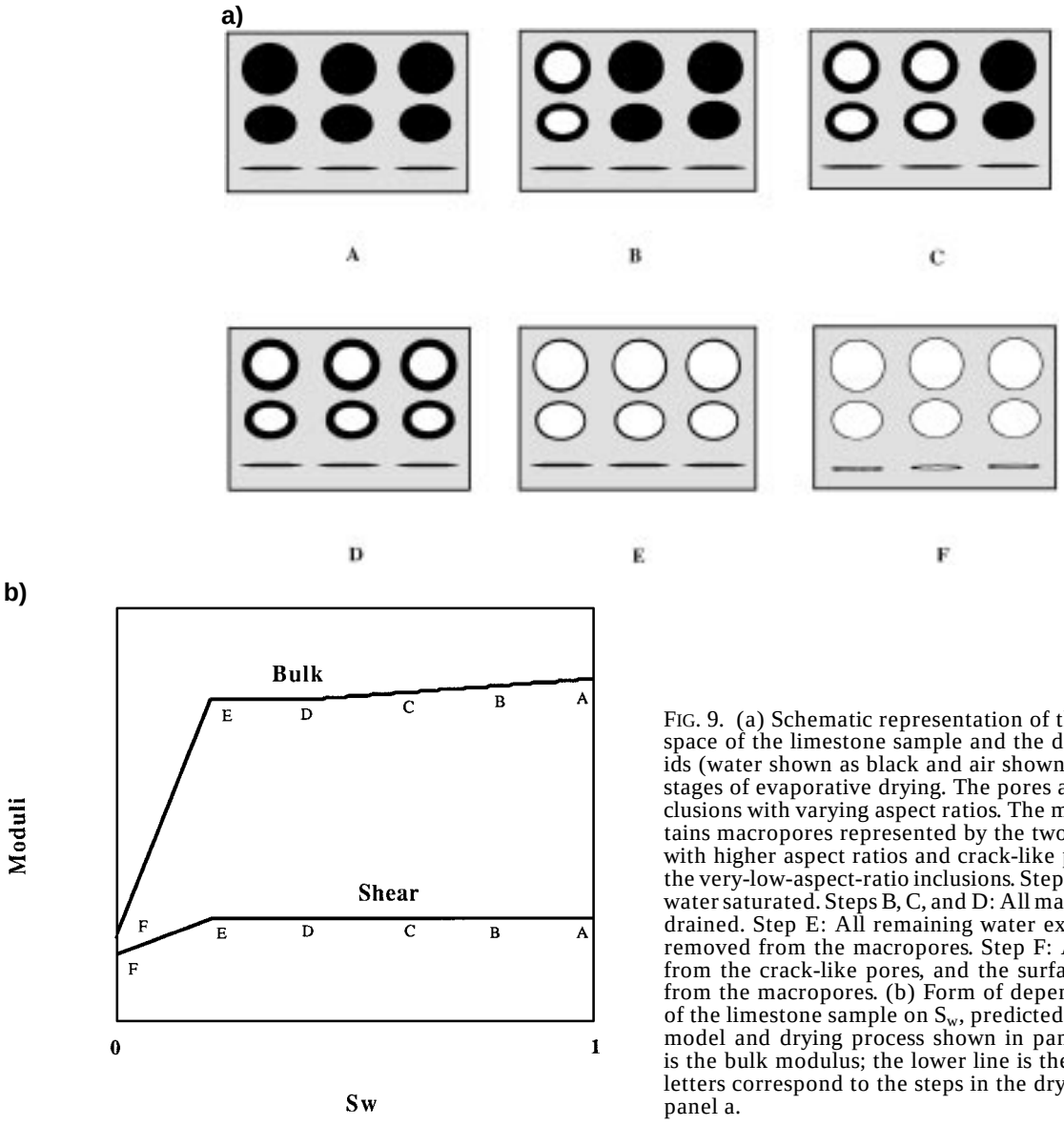

FIG. 9. (a) Schematic representation of the model of the pore space of the limestone sample and the distribution of the fluids (water shown as black and air shown as white) during the stages of evaporative drying. The pores are represented as inclusions with varying aspect ratios. The model pore space contains macropores represented by the two groups of inclusions with higher aspect ratios and crack-like pores represented by the very-low-aspect-ratio inclusions. Step A: All pores are fully water saturated. Steps B, C, and D: All macropores are partially drained. Step E: All remaining water except surface water is removed from the macropores. Step F: All water is removed from the crack-like pores, and the surface water is removed from the macropores. (b) Form of dependence of the moduli of the limestone sample on S_w, predicted using the pore-space model and drying process shown in panel a. The upper line is the bulk modulus; the lower line is the shear modulus. The letters correspond to the steps in the drying process shown in panel a.

The model results are in good qualitative agreement with the form of the data, which are distinctly different from the limestone data. In the limestone sample, the presence and drainage of crack-like geometries at low saturations within the falling rate period the dominant feature in the velocity data. The presence of the crack-like geometries thus results in a strong link between the drying rate data and the velocity data. The dolomite has no crack-like geometries. In this sample, pores with a range of aspect ratios drain at the higher saturations, primarily affecting the bulk modulus. The water that is removed at low saturations does not affect the moduli. Therefore, the falling rate period does not correspond to a saturation range over which there is a significant change in velocities.

Modeling the Berea data

The pore space of Berea sandstone is modeled by inclusions with a range of aspect ratios. The pores are represented by high- and intermediate-aspect-ratio inclusions, as in the case of Baker dolomite. The crack-like porosity evident at grain contacts is represented by very-low-aspect-ratio inclusions. The fluid distribution scenario during drying (Figure 11a) is displayed as involving six steps but can be divided into three main stages. Figure 11b shows the forms of the modulus-saturation relationships that are produced by this model.

In the first stage, which corresponds to the early stages of the constant rate period, the high- and intermediate-aspect-ratio pores sequentially and partially drain (steps A to D in Figure 11a). In this stage, the introduction of air into the pores causes a steady decrease in the bulk modulus and a gradual decrease in the shear modulus, as shown in Figure 11b between points A and D.

During the next stage, which lasts until the falling rate period, the saturation level of the partially drained pores is reduced to a low level (step E). The low saturation level is intended to represent the point at which the water within the pores becomes disconnected and is present in the surface roughness and as an adsorbed layer. The moduli (Figure 11b) stay approximately

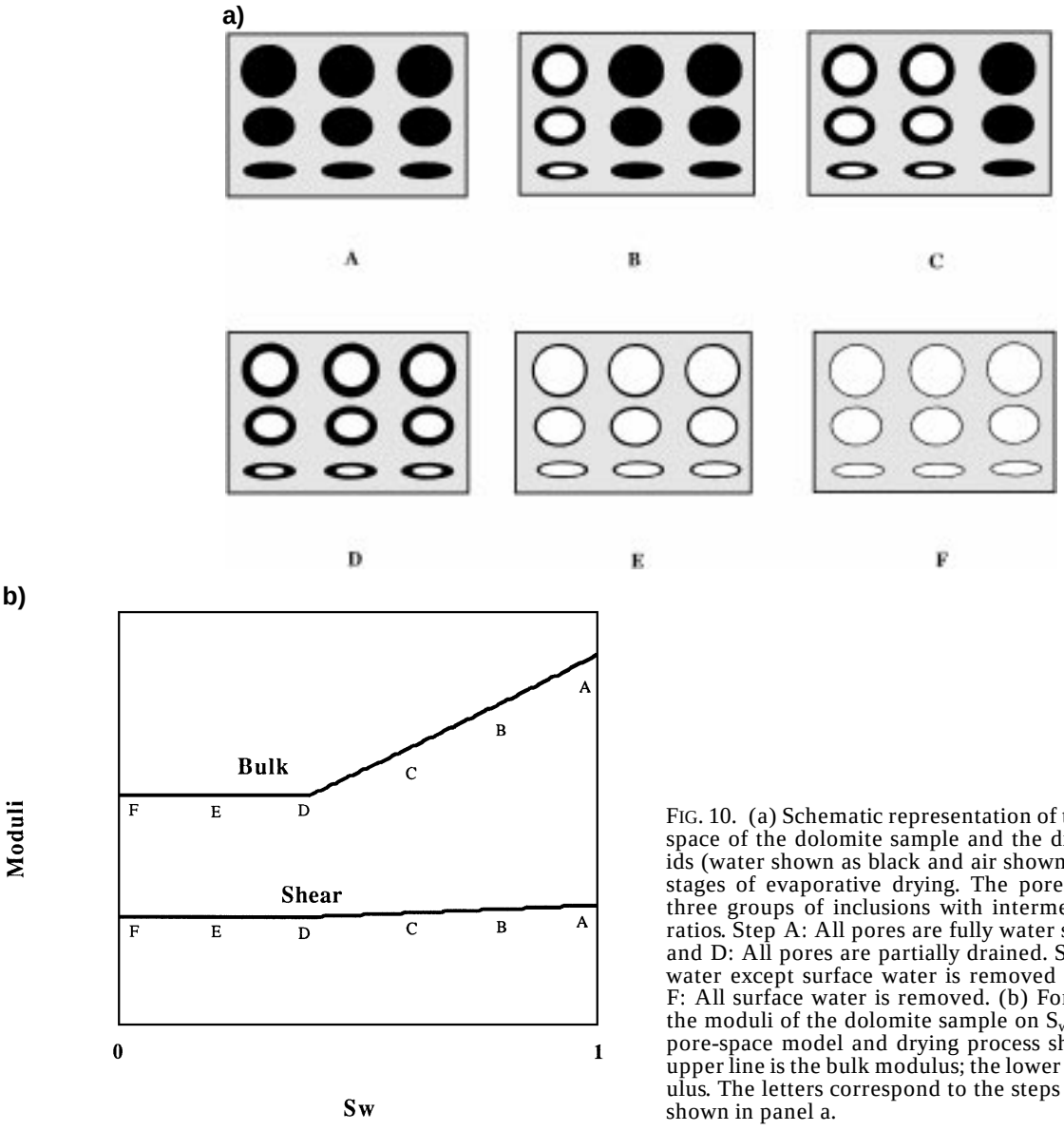

FIG. 10. (a) Schematic representation of the model of the pore space of the dolomite sample and the distribution of the fluids (water shown as black and air shown as white) during the stages of evaporative drying. The pores are represented as three groups of inclusions with intermediate to high aspect ratios. Step A: All pores are fully water saturated. Steps B, C, and D: All pores are partially drained. Step E: All remaining water except surface water is removed from the pores. Step F: All surface water is removed. (b) Form of dependence of the moduli of the dolomite sample on S_w, predicted using the pore-space model and drying process shown in panel a. The upper line is the bulk modulus; the lower line is the shear modulus. The letters correspond to the steps in the drying process shown in panel a.

constant between points D and E as the saturation level in the partially drained pores is reduced further.

Finally, during the third stage, the water on the surface and in the crack-like pores is drained (step F). In these last stages of drying, both the bulk and the shear moduli decrease sharply because of the removal of water from the crack-like pores and grain contact regions.

With regard to the form of the measured data, we see good agreement between the model and the variations in moduli and velocities at saturations above 0.15. At lower saturations, comparison of the model and data is complicated by rock-water interface effects. These effects will now be considered with reference to the differences seen in the drying and adsorption data for this sample.

Sandstone data at low saturations: Effects of sample-scale heterogeneity and rock-water interaction

At low saturations, we have two data sets for Berea sandstone. Let us first consider the adsorption data. Because adsorption occurred over six weeks but evaporative drying occurred over two days, the adsorption data are more likely to be representative of the response of the sample without the superimposed effects of sample-scale saturation heterogeneity. The decreases in bulk and shear moduli clearly seen in the adsorption data as water is added to the dry rock are attributed to the reduction in the surface free energy of the solid and the related reduction in contact adhesion. This same change in velocities in Berea sandstone when S_w is close to zero has been observed previously by Wyllie et al. (1962) and Pandit and King (1979).

As S_w is increased further through adsorption, both moduli show a dramatic increase until the point of maximum adsorption at $S_w = 0.15$. This is also the point at which the adsorption curve coincides with the drying curve. We attribute this increase to the stiffening of the system through the condensation of liquid water at grain contacts and in crack-like pores where water-air menisci have been established through the adsorption of surface layers of water. This model of the condensation of water in a porous material was originally proposed by Foster

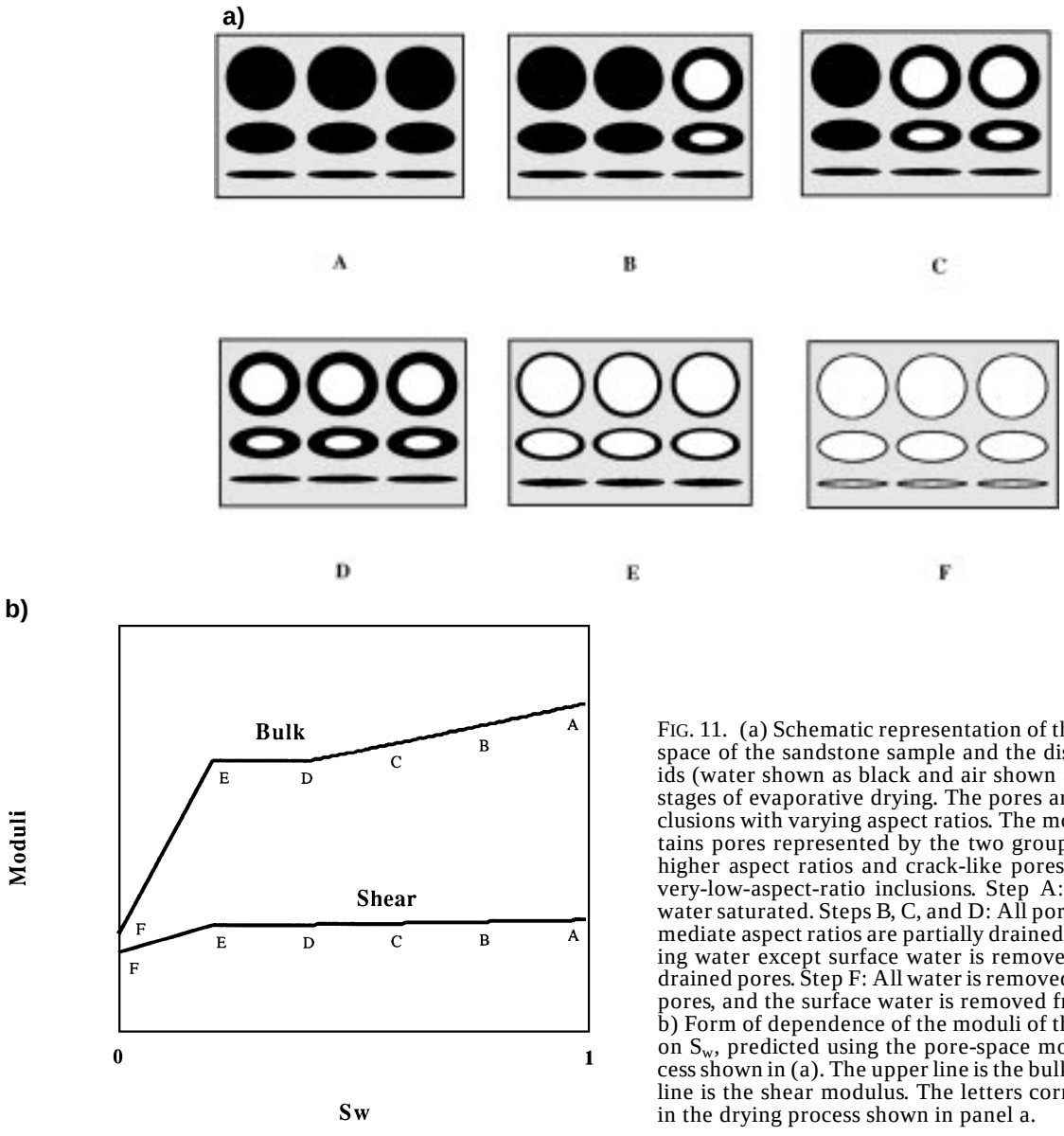

FIG. 11. (a) Schematic representation of the model of the pore space of the sandstone sample and the distribution of the fluids (water shown as black and air shown as white) during the stages of evaporative drying. The pores are represented as inclusions with varying aspect ratios. The model pore space contains pores represented by the two groups of inclusions with higher aspect ratios and crack-like pores represented by the very-low-aspect-ratio inclusions. Step A: All pores are fully water saturated. Steps B, C, and D: All pores with high to intermediate aspect ratios are partially drained. Step E: All remaining water except surface water is removed from the partially drained pores. Step F: All water is removed from the crack-like pores, and the surface water is removed from the other pores. b) Form of dependence of the moduli of the sandstone sample on S_w, predicted using the pore-space model and drying process shown in (a). The upper line is the bulk modulus; the lower line is the shear modulus. The letters correspond to the steps in the drying process shown in panel a.

(1932) and applied to partially saturated rocks by Knight and Nur (1987).

To gain insight into how the condensation proceeds, one can examine Kelvin's equation for vapor pressure P across a meniscus held in a cylindrical capillary, written as

$$P = P_0 \exp\left(\frac{\sigma v}{r R T}\right), \quad (8)$$

where P_0 is the ambient vapor pressure, σ is the surface tension in the meniscus, v is the molecular volume, r is the radius of curvature of the meniscus, R is the gas constant, and T is the temperature. From expression (8), it can be seen that menisci with smaller radii of curvature have a lower vapor pressure. Since the rate of condensation is proportional to the difference between the vapor pressure across the meniscus and the ambient vapor pressure, pores with a smaller radius will tend to be filled with liquid water before those with a larger radius. The adsorption process therefore will result in the saturation of a significant proportion of grain contacts and cracks. The saturation of these compliant regions results in the observed increases in both bulk and shear moduli.

A saturation level ($S_w = 0.15$) at which it was not possible to further increase S_w through adsorption was reached. It is interesting to note that this saturation level corresponds to the point at which the sharp increases in both the bulk and the shear moduli level off. In a constant-humidity environment, capillary condensation will cease when the radii of the menisci become large enough so that the vapor pressure across the interface is in equilibrium with the ambient vapor pressure. In the Berea sample, it appears that adsorption stops when a substantial amount of the crack-like porosity is saturated.

Let us now consider the data obtained during drying. We attribute the differences between the adsorption data and the drying data to the sample-scale saturation heterogeneities that are known to occur during the falling rate stage of drying. Specifically, we suggest that two competing effects occur in the sample during drying because the outside of the sample is at a lower saturation than the inside. In the outer regions of the sample, adsorbed surface water is being removed from grain contact areas, causing an increase in moduli. In the inner regions, water is being removed from the crack-like geometries, causing a decrease in moduli. That is, the bulk and shear moduli will increase toward the outside of the sample and decrease toward the inside of the sample as S_w in both regions decreases. The net result is that these two competing effects cause the measured form of the velocity-saturation relationship to depart significantly from what would be measured in a sample in which saturation is homogeneous. During the adsorption experiment conducted in this study, it appears that the more homogeneous saturation distribution makes it possible to resolve these two separate effects.

In summary, the form of the velocity data for Berea sandstone indicates a number of effects associated with the drying process and the geometry of the pore space. At higher saturations, throughout the constant rate period, a reduction in V_P and a subtle reduction in V_S correspond to the drainage of pores with a range of aspect ratios. Within the falling rate period, the removal of water from crack-like pores causes decreases in V_P and V_S. A second competing effect in the sandstone at these low saturations is caused by the rock-water interaction, which leads to an increase in V_P and V_S as S_w reaches zero. Resolving these two effects can be masked by saturation heterogeneity within the falling rate period.

CONCLUSIONS

This study has investigated the way in which the interaction between the microgeometry of the pore space and the drying process can influence the form of the velocity-saturation relationship. Elastic wave velocities and drying rates were measured in three different types of rock samples (limestone, dolomite, and sandstone) during evaporative drying. Drying rate curves were used to establish the start of the falling rate period, a transition that has been associated with the onset of the irreducible water saturation level within a drying sample. Velocity variations above this point were associated with the removal of water from the higher-aspect-ratio pores. In the falling rate period, velocity variations were associated with the removal of hydraulically disconnected water.

The most significant feature in the drying rate data and a very significant point in terms of the drying process is the start of the falling rate period. This study has shown that this key transition in the drying process, from hydraulically connected to disconnected water, results in a variable response in the velocity data. In samples with low-aspect-ratio regions of the pore space, e.g., the studied limestone and sandstone samples, we conclude that there will be a significant decrease in velocity when the hydraulically disconnected water is removed during the falling rate period. This result is of particular interest, as it suggests that detectable velocity variations may be associated specifically with the approach of a sample to the irreducible saturation level. Velocity measurements could prove to be useful in the laboratory as a means of characterizing the geometry of the pore space retaining water at low saturations. Further studies are required to determine if this velocity effect persists at lower frequencies. If so, there could be a sonic or seismic indicator of irreducible saturation.

Using petrographic information and the form of the drying rate data, simple models of the pore-space microgeometry and the drying process were used to model the velocity data. The good agreement in the form of the models and data suggests that a simple analysis of drying rates and pore-space microgeometries can be very useful in interpreting the form of the velocity-saturation relationship.

ACKNOWLEDGMENTS

This research was supported primarily by funding to R. Knight from Imperial Oil, Petro-Canada, Shell Canada, and an Industrially Oriented Research Grant from the Natural Sciences and Engineering Research Council of Canada (NSERC). Additional funding was provided by an NSERC Research Grant. Funding to purchase the equipment for the measurement of elastic wave velocities was obtained from an NSERC Equipment Grant. We thank Gary Mavko for reading this paper and for helpful comments. We also thank Wayne Pennington for review and handling of this paper as Associate Editor.

REFERENCES

Born, W. T., and Owen, J. E., 1935, Effect of moisture on velocity of elastic waves in Amherst sandstone: Am. Assoc. Pet. Geol. Bull., **19**, 9–18.

Cadoret, T., Marion, D., and Zinszner, B., 1992a, 1 kHz elastic wave velocities in partially saturated limestones: Evidence of fluid distribution effects: 62nd Ann. Internat. Mtg., Soc. Expl. Geophys., Expanded Abstracts, 658–661.

———1992b, Sonic wave velocity and X-ray tomography images for partially saturated rocks: Evidence of microscopic fluid distribution effect on acoustic properties: Presented at the 3rd Euro. Core Anal. Symp.: Euro. Soc. Core Analysts.

———1993, The influence of frequency and fluid distribution on acoustic velocities in partially saturated limestones: 63rd Ann. Internat. Mtg., Soc. Expl. Geophys., Expanded Abstracts, 782–785.

Clark, V. A., Tittman, B. R., and Spencer, T. W., 1980, Effect of volatiles on attenuation (Q) and velocities in sedimentary rocks: J. Geophys. Res., **85**, 5190–5198.

Endres, A. L., and Knight, R., 1989, The effect of microscopic fluid distribution on elastic wave velocities: The Log Analyst, **30**, 437–445.

Endres, A. L., and Knight, R. J., 1991, The effects of pore scale fluid distribution on the physical properties of partially saturated tight sandstones: J. Appl. Physics, **69**, 1091–1098.

Foster, G., 1932, The sorption of condensible vapors by porous solids, Part I. The applicability of capillary theory: Trans. Faraday Soc., **28**, 645–657.

Guillot, G., Trokiner, A., Darrasse, L., and Sainte-Jalmes, H., 1989, Drying of a porous rock monitored by NMR imaging: J. Phys. D, **22**, 1646–1649.

Keey, R. B., 1972, Drying principles and practice: Pergamon Press, Inc.

Knight, R. J., and Dvorkin, J., 1992, Seismic and electrical properties of sandstone at low saturations: J. Geophys. Res., **97**, 17 425–17 432.

Knight, R. J., and Nolen-Hoeksema, R., 1990, A laboratory study of the dependence of elastic wave velocities on pore scale fluid distribution: Geophys. Res. Lett., **17**, 1529–1532.

Knight, R. J., and Nur, A., 1987, Geometrical effects in the dielectric response of partially saturated sandstones: The Log Analyst, **28**, 513–519.

Kuster, G. T., and Toksöz, M. N., 1974, Velocity and attenuation of seismic waves in two phase media. I. Theoretical formulations: Geophysics, **39**, 587–606.

Mavko, G., and Jizba, D., 1991, Estimating grain-scale fluid effects in velocity dispersion in rocks: Geophysics, **56**, 1940–1949.

Mavko, G., and Nur, A., 1979, Wave attenuation in partially saturated rocks: Geophysics, **44**, 161–178.

Murphy, W. F., Winkler, K. W., and Kleinberg, R. L., 1984, Frame modulus reduction in sedimentary rocks: The effect of adsorption at grain contact: Geophys. Res. Lett., **11**, 805–808.

———1986, Acoustic relaxation in sedimentary rocks: Dependence on grain contacts: Geophysics, **51**, 757–766.

O'Connell, R., and Budiansky, B., 1974, Seismic velocities in dry and saturated cracked solids: J. Geophys. Res., **79**, 5412–5426.

———1977, Viscoelastic properties of fluid-saturated cracked solids: J. Geophys. Res., **82**, 5719–5735.

Pandit, B. I., and King, M. S., 1979, The variation of elastic wave velocities and quality factor Q of a sandstone with moisture content: Can. J. Earth Sci., **16**, 2187–2195.

Toksöz, M. N., Cheng, C. H., and Timur, A., 1976, Velocities of seismic waves in porous rocks: Geophysics, **41**, 621–645.

van Brakel, J., 1980, Mass transfer in convective drying, *in* Mujumdar, A. S., Ed., Advances in drying: Hemisphere Publ. Corp., 217–267.

Walsh, J. B., 1965, The effects of cracks on the compressibility of rock: J. Geophys. Res., **70**, 381–389.

Whitaker, S., 1985, Moisture transport mechanisms during the drying of granular porous media, *in* Toei, R., and Mujumdar, A. S., Eds., Drying '85: Hemisphere Publ. Corp., 21–32.

Wilks, K. W., and Tercier, P., 1993, Sample descriptions, rock physics research program, Vol. 2: Univ. of British Columbia.

Winkler, K. W., 1985, Dispersion analysis of velocity and attenuation in Berea sandstones: J. Geophys. Res., **88**, 9493–9499.

Wyllie, M. R. J., Gregory, A. R., and Gardner, G. H. F., 1962, Studies of elastic wave attenuation in porous media: Geophysics, **27**, 569–589.